Published in final edited form as:
Sci Signal. ; 3(145): ra77. doi:10.1126/scisignal.2001200.

Antagonistic Regulation of Actin Dynamics and Cell Motility by TRPC5 and TRPC6 Channels

Dequan Tian[1,*], **Sarah M. P. Jacobo**[1,*], **David Billing**[1], **Anete Rozkalne**[1], **Steven D. Gage**[1], **Theodora Anagnostou**[1], **Hermann Pavenstädt**[2], **Hsiang-Hao Hsu**[3], **Johannes Schlondorff**[4], **Arnolt Ramos**[1], and **Anna Greka**[1,†]

[1] Harvard Medical School and Massachusetts General Hospital, Boston, MA 02114, USA

[2] Medizinische Klinik und Poliklinik D, 48149 Muenster, Germany

[3] Chang Gung Memorial Hospital and University, Taoyuan 333, Taiwan

[4] Beth Israel Deaconess Medical Center, Boston, MA 02115, USA

Abstract

The Rho family of small guanosine triphosphatases (Rho GTPases: RhoA, Cdc42, and Rac1) regulates many aspects of cell behavior, including actin dynamics and cell migration. The generation of calcium ion (Ca^{2+}) microdomains is critical in promoting cell migration because they control the localized activity of Rho GTPases. We identified receptor-activated TRPC5 and TRPC6 (transient receptor potential canonical type 5 and 6) channels as antagonistic regulators of actin remodeling and cell motility in fibroblasts and kidney podocytes. We show that TRPC5 is in a molecular complex with Rac1, whereas TRPC6 is in a molecular complex with RhoA. TRPC5-mediated Ca^{2+} influx induces Rac1 activation, thereby promoting cell migration, whereas TRPC6-mediated Ca^{2+} influx increases RhoA activity, thereby inhibiting cell migration. Our data unveil antagonistic Ca^{2+} influx pathways as a conserved signaling mechanism for the integrated regulation of cell migration.

INTRODUCTION

Ca^{2+}-dependent remodeling of the actin cytoskeleton is a dynamic process that drives cell migration (1,2) through modulation of the activity of members of the Rho family (RhoA, Cdc42, Rac1) of small guanosine triphosphatases (GTPases) (3–6). At the leading edge,

†To whom correspondence should be addressed. greka.anna@mgh.harvard.edu.
*These authors contributed equally to this work.

Author contributions: D.T., S.M.P.J., D.B., S.D.G., A. Ramos, A. Rozkalne, T.A., and A.G. performed the experiments; D.T., S.M.P.J., S.D.G., and A.G. analyzed the data; H.-H.H., H.P., and J.S. provided the reagents; A.G. designed the experiments, supervised the project, and wrote the paper.

Competing interests: U.S. patent “TRPC5 channels in proteinuric kidney disease” pending (A.G.).

SUPPLEMENTARY MATERIALS
www.sciencesignaling.org/cgi/content/full/3/145/ra77/DC1
Fig. S1. Ang II–evoked TRPC-like currents in podocytes.
Fig. S2. Gene silencing of TRPC channels in a lentiviral delivery system.
Fig. S3. Ca^{2+} imaging and patch-clamp electrophysiology in TRPC-depleted podocytes.
Fig. S4. Ang II–induced TRPC5 and TRPC6 activation has antagonistic effects on the actin cytoskeleton in wild-type podocytes.
Fig. S5. TRPC gene silencing in podocytes and antibody validation.
Fig. S6. Colocalization of TRPC5 with Rac1 and TRPC6 with RhoA in podocytes.
Fig. S7. Rac1 mediates increased Ang II–dependent TRPC5 insertion into the plasma membrane.
Fig. S8. Podocytes at the edge of the wound display characteristic actin phenotypes.

Rac1 and Cdc42 promote cell motility through the formation of lamellipodia and filopodia, respectively (4). In contrast, RhoA promotes the formation of stress fibers and focal contacts, generating a contractile phenotype (4). Spatially and temporally restricted changes in the concentration of free calcium (Ca^{2+} flickers) are enriched near the leading edge of migrating cells (2). Recent studies have implicated mechanically activated channels in the generation of Ca^{2+} flickers that steer cell migration (7). Ca^{2+} microdomains are thought to promote cell migration, but little is known about inhibition of cell motility by antagonistic Ca^{2+} influx pathways.

Receptor-activated TRPC (transient receptor potential canonical) channels generate Ca^{2+} microdomains in many cell types (7–11), but cross talk between these channels in the regulation of cell migration has not been described. Specifically, TRPC5 channels generate Ca^{2+} transients implicated in neuronal growth cone motility (8,12) and vascular smooth muscle cell migration (13), but their downstream targets are largely unknown. TRPC6 channels, which restrict endothelial cell migration (14), have been implicated in pulmonary arterial hypertension (15), cardiac hypertrophy, and fibrosis (16–19). TRPC6 dysfunction is also linked to human genetic kidney disease (20,21), but the specific mechanisms through which these channels act remain elusive.

Fibroblasts are mesenchymal cells with the ability to assume a motile phenotype for processes such as wound healing (4). Podocytes, which are pericyte-like cells covering the outer aspect of glomerular capillaries, have a contractile apparatus essential for the maintenance of the kidney filtration barrier (22,23). Podocytes respond to environmental cues through an exquisitely refined repertoire of cytoskeletal adaptations (22–28), which renders them an ideal model system to study actin dynamics in a physiologic context. Early podocyte injury is characterized by dysregulation of Ca^{2+} homeostasis (29,30) followed by disruption of the actomyosin contractile apparatus (23,31,32), suggesting a link between Ca^{2+} influx and cytoskeletal reorganization. These events in podocytes have been correlated with proteinuric kidney disease, the loss of protein in the urine, and, ultimately, kidney failure (30,33–35). Specifically, recent work has shown that the RhoA-mediated preservation of the actomyosin contractile apparatus in podocytes results in preservation of stress fibers in vitro and the kidney filtration barrier in vivo (30,32), whereas the activation of Cdc42 and Rac1 was correlated with proteinuria (35,36). Here, we show that the receptor-activated TRPC5 and TRPC6 channels trigger antagonistic pathways of cytoskeletal remodeling in podocytes and fibroblasts. These data extend the traditional view of the role of Ca^{2+} transients in cell migration by showing that the conserved, antagonistic, and mutually inhibitory pathways triggered by TRPC5 and TRPC6 are critical regulators of cell migration through differential coupling to Rac1 and RhoA, respectively.

RESULTS

TRPC5 and TRPC6 channels mediate angiotensin II–induced Ca^{2+} influx

TRPC channels are typically activated through heterotrimeric guanosine 5′-triphosphate–binding protein (G protein)–coupled receptors (GPCRs) that signal through G_q (9). We identified the angiotensin type 1 receptor (AT1R) as a pertinent upstream activator of TRPCs (fig. S1). Wild-type podocytes, which have a low density of AT1Rs (37), produced only occasional, statistically unreliable global Ca^{2+} transients in response to angiotensin II (Ang II). Stimulation of a podocyte line with stable overexpression of the AT1R (AT1R podocytes) with Ang II (500 nM) resulted in robust Ca^{2+} transients (fig. S1A). The AT1R antagonist losartan (200 nM) diminished the amplitude of the Ca^{2+} transient by >70% (fig. S1B). Patch-clamp electrophysiology in the whole-cell configuration revealed that Ang II (500 nM) evoked a TRP-like current with reversal potential at 0 mV, a small inward component, and steep outward rectification at positive potentials (fig. S1C). Although TRPV

and TRPM (TRP vanilloid and metastatin, respectively) currents could not be excluded, the observed current-voltage (*I*–*V*) relationship was consistent with those of TRPC-like currents (9). The normalized peak current was 10 ± 4 pA/pF at −100 mV and 20 ± 7 pA/pF at +100 mV (fig. S1D).

To investigate the molecular identity of this Ang II–evoked current, we performed reverse transcription polymerase chain reaction (RT-PCR) with messenger RNA (mRNA) from wild-type or AT1R podocytes; this revealed transcripts for TRPC1, TRPC5, TRPC6, and TRPC7 in both wild-type and AT1R podocytes (fig. S2A). Next, we pursued a gene-silencing approach to identify the channels contributing to the recorded TRPC-like current. Using a lentiviral system, we silenced each TRPC channel with 80 to 90% efficiency, as assayed by RT-PCR (fig. S2B). We reasoned that gene silencing of channel subunits essential for Ang II–evoked Ca^{2+} influx into podocytes would reduce the peak amplitude of the Ca^{2+} transients relative to those in unsilenced controls. In initial Ca^{2+}-imaging experiments, only TRPC5- or TRPC6-depleted cells showed a statistically significant reduction in the peak amplitude of the Ca^{2+} transients as compared to controls that received scrambled short hairpin RNA (shRNA) or TRPC1-, TRPC4-, or TRPC7-depleted cells (Fig. 1 and fig. S3, A to C). We confirmed the efficiency of gene silencing of TRPC5 and TRPC6 at the protein level by Western blot analysis of podocyte lysates from control versus TRPC5- or TRPC6-silenced cells (fig. S2C). In Ca^{2+} add-back experiments, in which cells were first exposed to Ang II in the absence of Ca^{2+} and then reexposed in its presence, Ang II–mediated release of Ca^{2+} from internal stores (0 mM Ca^{2+} bath) was significant, and subsequent responses in the presence of 2 mM Ca^{2+} were commonly seen (Fig. 1). However, in the presence of shRNA directed against TRPC5 or TRPC6, the Ca^{2+} response after addition of 2 mM Ca^{2+} to the bath was significantly diminished by 60 and 50%, respectively (Fig. 1, E to H). This suggests that Ca^{2+} entry mechanisms in podocytes are in part mediated by TRPC5 and TRPC6 channels. Together, these data point to TRPC5 and TRPC6, but not TRPC1, TRPC4, or TRPC7, as the likely pore-forming subunits that contribute to Ang II–evoked Ca^{2+} influx in podocytes. Because TRPC5 subunits are not likely to oligomerize with TRPC6 (38), our results suggest that, in podocytes, the putative Ca^{2+} conduction pores consist of homomeric TRPC5 and TRPC6 channels.

Single-channel recordings reveal TRPC5- and TRPC6-like conductances

To identify endogenous TRPC channels at the single-channel level, we performed recordings in the outside-out configuration. A step voltage protocol after bath perfusion with Ang II revealed native TRPC-like channels with small-amplitude inward current at negative potentials, reversal of the current to the outward direction at 0 mV, and increased amplitude at positive potentials (fig. S1E). In a representative patch, the application of Ang II at V_{step} +100 mV revealed three populations of channels with the corresponding unitary conductances: (G1) 39 pS, (G2) 68 pS, and (G3) 80 pS (Fig. 2, A to C). Given that TRPC5 and TRPC6 channels have virtually identical single-channel conductances [that of TRPC5 has been variably reported as 25 to 38 pS and that of TRPC6 as 25 to 44 pS (9,39–44)], we applied lanthanum (La^{3+}), which blocks TRPC6 (9) and increases the open-channel probability of TRPC5 (45), to distinguish between the two. Application of La^{3+} (100 μM) unmasked a distinct conductance (G4) at 33 pS (Fig. 2B). Removal of La^{3+} from the bath solution restored conductances (G1), (G2), and (G3) (Fig. 2C). Analysis of this patch, which was representative of recordings obtained from five cells, revealed unitary conductances corresponding to a population of three active channels consisting of a single TRPC5 channel and two TRPC6 channels. (G1) of 39 pS represented the average conductance when a single channel, either TRPC5 or TRPC6, opened in response to Ang II. When TRPC5 and TRPC6 were open simultaneously, their current summation yielded conductance (G2) of 68 pS. Conductance (G3) was mediated by the summation of two TRPC6 channels (Fig. 2A).

Application of La^{3+} blocked the TRPC6 conductances and revealed the TRPC5 conductance (G4) at 33 pS (Fig. 2B). Together, these single-channel data identify native TRPC5- and TRPC6-like conductances in podocytes.

As an additional control, we overexpressed wild-type TRPC5 and TRPC6 in podocytes, using a lentiviral expression system, and performed outside-out recordings under the same conditions as those used for recordings from endogenous channels. Podocytes overexpressing wild-type TRPC5 had a brisk response to Ang II, with a single-channel conductance (G5) that correlated well with the single-channel conductance of endogenous TRPC5-like channels recorded in previous experiments [(G4) in Fig. 2B versus (G5) in Fig. 2, D, trace 1, and F]. This conductance was potentiated by the application of La^{3+} (Fig. 2, D, trace 2, and F). Podocytes overexpressing wild-type TRPC6 responded to Ang II with a conductance that correlated well with that recorded for endogenous TRPC6-like channels [(G1) in Fig. 2A, which was the overlap of TRPC5 and TRPC6, compared with (G7) in Fig. 2, E, trace 1, and G]. La^{3+} abolished channel activity in these patches (Fig. 2E, trace 2). Finally, we conducted gene-silencing analyses for TRPC5 and TRPC6. Gene silencing of TRPC6 channels resulted in unstable patches, preventing single-channel recordings. TRPC5 depletion abrogated TRPC5 channel activity in podocytes overexpressing wild-type TRPC5 and TRPC6 (fig. S3G). In a representative patch ($n = 6$ cells), the application of La^{3+} revealed no channel activity, indicating that the single-channel conductances elicited by Ang II were mediated by TRPC6 channels (fig. S3G). TRPC6-like conductances were restored after removal of La^{3+} from the bath (fig. S3G). Together, the single-channel data reveal the presence of TRPC5 and TRPC6 channels in podocytes.

TRPC5 and TRPC6 mediate distinct actin phenotypes

Given that Ang II–mediated Ca^{2+} influx has been linked to cytoskeletal changes (37), we tested for specific effects of TRPC5 and TRPC6 activity on the actin cytoskeleton. To isolate the effects of AT1R-induced TRPC modulation of the cytoskeleton from possible effects of constituents of serum in the cell culture medium, we serum-starved podocytes for 3 hours before exposure to Ang II or serum. As previously described, serum-starved wild-type (32) and AT1R (37) podocytes showed prominent stress fibers (fig. S4A). Exposure of wild-type podocytes to Ang II led to a decrease in stress fibers and the reorganization of actin into cortical rings or arcs (fig. S4A) (37). This phenotype was more prominent in serum-treated cells, indicating that a combination of growth factors present in serum activates pathways that collectively modulate podocyte actin organization (fig. S4A). Similar actin arcs have been described in many cell types, including AT1R podocytes, where they correlate with a motile cell phenotype (37). Exposure of wild-type or AT1R cells to Ang II induced prominent actin arcs (fig. S4A). Treatment with the AT1R antagonist losartan (200 nM) before Ang II exposure prevented reorganization into the arc phenotype and preserved stress fibers (fig. S4A).

We next determined whether Ang II–mediated reorganization of the actin cytoskeleton in podocytes involved TRPC5 or TRPC6. Gene silencing of TRPC5 or TRPC6 had no effect on the actin cytoskeleton of podocytes in the absence of Ang II treatment, showing prominent stress fibers similar to non–Ang II–treated scrambled shRNA–expressing or wild-type cells (fig. S4, A and B). However, Ang II treatment of TRPC6-depleted (C6 shRNA) AT1R or wild-type podocytes resulted in loss of stress fibers [AT1R: 15 ± 2 versus 5 ± 1; wild type: 18 ± 2 versus 4 ± 1; one-way analysis of variance (ANOVA), Fisher's least significant difference (LSD), $P < 0.001$, $n = 50$ cells] (Fig. 3, A and B, and fig. S4, C and D). Paxillin staining was also significantly reduced in TRPC6-depleted cells treated with Ang II, indicating a reduction in focal adhesions (AT1R: 30 ± 4 versus 10 ± 1; wild type: 35 ± 5 versus 5 ± 2) (Fig. 3, A and C, and fig. S4, C and E). In contrast, Ang II treatment of TRPC5-depleted (C5 shRNA) AT1R and wild-type podocytes restored stress fibers (AT1R:

15 ± 2 versus 25 ± 4; wild type: 18 ± 2 versus 21 ± 2; one-way ANOVA, Fisher's LSD, $P < 0.05$ to 0.001, $n = 50$ cells) (Fig. 3, A and B, and fig. S4, C and D). TRPC5-depleted cells treated with Ang II also showed restored focal adhesions located throughout the cell relative to TRPC6-depleted cells (AT1R: 10 ± 1 versus 45 ± 5; wild type: 5 ± 2 versus 35 ± 2; one-way ANOVA, Fisher's LSD, $P < 0.01$, $n = 50$ cells) (Fig. 3, A and C, and fig. S4, C and E). Gene silencing of TRPC1 or TRPC7 (C1 shRNA or C7 shRNA) had no effect on the actin cytoskeleton of cells treated with Ang II (fig. S5A). RT-PCR analysis showed that neither TRPC5 nor TRPC6 transcript abundance significantly changed upon silencing of the counterpart channel (fig. S2, D to G). This suggests that the observed phenotypes were not related to up-regulation of one channel in the absence of another, as seen for TRPC channels in other experimental settings (46). Moreover, immunolocalization experiments revealed that neither TRPC5 nor TRPC6 membrane abundance was affected by silencing of the counterpart channel (fig. S5B, middle). These data suggest that endogenous TRPC6 maintains a contractile, stationary cell phenotype upon Ang II stimulation, whereas endogenous TRPC5 suppresses stress fiber and focal adhesion formation, thereby promoting a motile phenotype.

Functional coupling between TRPCs and Rho GTPases regulates the actin cytoskeleton

Given the observed actin phenotypes, we next investigated whether TRPC5 and TRPC6 are differentially coupled to signal transduction pathways that maintain the balance between contractility and motility. RhoA enhances contractility and, through a mechanism of reciprocal inhibition, Rac1 enhances motility, with both contributing to cytoskeletal homeostasis (4,5). We hypothesized that Ang II–activated TRPC5 stimulates an increase in the abundance of active, guanosine triphosphate (GTP)–bound Rac1, whereas TRPC6 stimulates an increase in the abundance of active, GTP-bound RhoA. To test this hypothesis, we performed in vitro GTPase assays in human embryonic kidney (HEK) cells coexpressing the AT1R and TRPC channels (Fig. 3, D to F). Total lysates from Ang II–stimulated cells were affinity-isolated with either p21-activated kinase (PAK1) or Rhotekin, which bind active, GTP-bound Rac1 or RhoA, respectively (4). Coexpression of AT1R and TRPC5 in HEK cells increased activated Rac1 relative to that in cells expressing AT1R alone (Fig. 3D, lane 2 versus lane 1). In contrast, coexpression of AT1R and TRPC6 increased activated RhoA and decreased activated Rac1 relative to AT1R alone (lane 3 versus lane 1). The abundance of active RhoA was reduced by the coexpression of AT1R and TRPC5 (lane 2). Together, these data suggest a functional dependence of Rac1 on TRPC5 channel activity, and of RhoA on TRPC6 channel activity.

Next, we explored the molecular mechanisms through which functional coupling of TRPC5 to Rac1 and TRPC6 to RhoA might occur. We performed coimmunoprecipitation experiments, using total lysates from HEK cells expressing TRPC5–green fluorescent protein (GFP) or TRPC6-GFP. Lysates were affinity-isolated for either Rac1-GTP (by binding to PAK1 agarose) or RhoA-GTP (by binding to Rhotekin agarose), and Western blots were performed (Fig. 3G). Relative to TRPC6-GFP, Rac1-GTP coimmunoprecipitated preferentially with TRPC5-GFP (upper panel), whereas RhoA-GTP coimmunoprecipitated preferentially with TRPC6-GFP (middle panel). Double immunolabeling analyses confirmed partial colocalization of TRPC5 with Rac1 (fig. S6), and TRPC6 with RhoA (fig. S6). These data suggest that Rac1 and TRPC5 are frequently found in the same molecular complex and that RhoA is present with TRPC6 in a distinct molecular complex.

To investigate the membrane localization patterns of TRPC5 and TRPC6 channels in podocytes, we performed immunocytochemistry experiments using antibodies directed against TRPC5 or TRPC6. In control (scrambled shRNA) cells, TRPC5 and TRPC6 localized to the plasma membrane in distinct puncta and were also present in a granular cytoplasmic distribution (Fig. 4A). High-power images showed discrete localization of

green (TRPC6) and red (TRPC5) puncta on the cell membrane (Fig. 4A). Quantification of green versus red puncta in randomly selected areas of the membrane revealed a 60 to 35% distribution of TRPC6-labeled puncta versus TRPC5-labeled puncta (Fig. 4B). This pattern of TRPC6 predominance on the podocyte plasma membrane persisted after treatment with Ang II or losartan and in the presence of constitutively active RhoA (CA RhoV12). However, in the presence of constitutively active Rac1 (CA RacV14), plasma membrane TRPC5 predominated over TRPC6. The Rac1-mediated translocation of TRPC5 to the membrane was consistent with previous studies (12) (one-way ANOVA, $P < 0.001$; $n = 20$ cells). Quantification of puncta in which TRPC5 and TRPC6 labeling was merged, generating yellow puncta, revealed minimal colocalization under all conditions tested (Fig. 4B, yellow bars), suggesting that TRPC5 and TRPC6 predominantly localize to discrete membrane compartments. Quantification of the total number of puncta present in a standard length of membrane revealed that Ang II, losartan, and CA RhoV12 had no effect on the total number of membrane TRPC channels (Fig. 4C). Consistent with previous studies (12), CA RacV14 increased the total number of puncta in the membrane (Fig. 4C).

Biotinylation studies of HEK cells coexpressing the AT1R and TRPC5-GFP or TRPC6-GFP revealed unchanged membrane abundance of TRPC6 after treatment with Ang II (fig. S7A). Coexpression of TRPC5-GFP or TRPC6-GFP with CA RacV14 resulted in increased Ang II–mediated membrane abundance for TRPC5, in keeping with the immunolocalization experiments (fig. S7A) (12). Coexpression with CA RhoV12 resulted in sustained abundance for both channels in the presence of Ang II (fig. S7A).

To test for functional effects of Rac1 and RhoA on TRPC5 and TRPC6 channels, we performed outside-out patch recordings in podocytes expressing CA RacV14 or CA RhoV12. In control recordings (fig. S7B; $n = 4$ cells), Ang II evoked single-channel conductances consistent with those seen previously (Fig. 2), and TRPC5 channel activity was increased by co-application of La^{3+}. In cells expressing CA RacV14 (fig. S7C; $n = 6$ cells), the number of channels was increased by a factor of 4; co-application of La^{3+} revealed that TRPC5 channels largely accounted for this increase, consistent with the biotinylation and immunolocalization analyses (figs. S4 and S7A) (12). Increased episodes of current summation were observed in the presence of CA RhoV12, suggesting enhanced channel insertion in these patches, consistent with the sustained channel abundance observed in the biotinylation experiments (fig. S7A). Overall, however, TRPC6 channel activity predominated in cells expressing CA RhoV12; application of La^{3+} unmasked only a modest contribution from TRPC5 channels. These data reveal that Rac1 is associated predominantly with TRPC5 activity in the podocyte plasma membrane, whereas RhoA is associated predominantly with TRPC6 activity.

We next verified the functional coupling between TRPC5 and Rac1 and TRPC6 and RhoA in podocytes. Dominant-negative RhoA (DN RhoN19) elicits loss of stress fibers, whereas dominant-negative Rac1 (DN RacN17) promotes stress fiber formation (4). Conversely, constitutively active RhoA (CA RhoV14) promotes stress fiber formation, whereas constitutively active Rac1 (CA RacV12) elicits loss of stress fibers (4). Consistent with previous studies, DN RhoN19 and CA RacV12 induced loss of stress fibers, and DN RacN17 and CA RhoV14 promoted stress fiber formation (Fig. 5A). Introduction of a dominant-negative pore mutant of TRPC5 (47) phenocopied the TRPC5-depleted phenotype, suggesting that loss of ion permeation through the TRPC5 channel is responsible for the cytoskeletal changes in TRPC5-silenced podocytes (Fig. 5A). Overexpression of DN RhoN19 in TRPC5-depleted podocytes abolished stress fibers (22 ± 3 versus 4 ± 1; one-way ANOVA, Fisher's LSD, $P < 0.001$; $n = 60$ cells), phenocopying TRPC6-silenced cells (Fig. 5, A and B). Introduction of wild-type TRPC5 in TRPC5-depleted cells restored near-maximal Ca^{2+} transient amplitude in Ca^{2+}-imaging experiments (fig. S3, D and F) and

induced loss of stress fibers (22 ± 3 versus 6 ± 1) (Fig. 5, A and B). Overexpression of CA RacV12 reversed the dominant-negative TRPC5 phenotype (27 ± 1 versus 7 ± 1) (Fig. 5, A and B). In contrast, introduction of a dominant-negative pore mutant of TRPC6 (47) phenocopied the TRPC6-depleted phenotype, suggesting that loss of ion permeation through the TRPC6 channel is responsible for the cytoskeletal changes in TRPC6-silenced podocytes (Fig. 5A). Overexpression of DN RacN17 restored stress fibers in TRPC6-silenced cells (21 ± 2 versus 3 ± 1) (Fig. 5, A and B). Expression of wild-type TRPC6 in the silenced TRPC6 background restored near-maximal Ca^{2+} transient amplitude in Ca^{2+}-imaging experiments (fig. S3, E and F) and also restored stress fibers (21 ± 3 versus 3 ± 1) (Fig. 5, A and B). Overexpression of CA RhoV14 rescued the dominant-negative TRPC6 phenotype, inducing stress fiber formation (27 ± 1 versus 6 ± 1) (Fig. 5, A and B). Notably, TRPC5-silenced cells phenocopied cells pretreated with losartan (23 ± 2 and 25 ± 1) (Fig. 5B). Together, these data imply an antagonistic relationship between the TRPC5-Rac1 and TRPC6-RhoA molecular complexes. The reversal of the dominant-negative TRPC5 phenotype by CA RacV12 suggests that Ca^{2+} influx through TRPC5 is upstream of Rac1 signaling. Similarly, the reversal of the dominant-negative TRPC6 phenotype by CA RhoV14 suggests that Ca^{2+} influx through TRPC6 is upstream of RhoA signaling.

RhoA signaling in podocytes is regulated by synaptopodin (32), a proline-rich, actin-associated protein found in highly dynamic cell compartments including dendritic spines in the brain and podocyte foot processes in the kidney (48). Furthermore, calcineurin-dependent degradation of synaptopodin leads to proteinuria in mice, and the calcineurin inhibitor cyclosporine A (CsA) protects against proteinuria by blocking the synaptopodin degradation (30). We therefore investigated the effects of TRPC5 and TRPC6 gene silencing on synaptopodin abundance. In control podocytes (scrambled shRNA), synaptopodin was found abundantly in the characteristic punctate distribution along actin stress fibers (Fig. 6A). Treatment of control cells with Ang II resulted in significant reduction in the abundance of synaptopodin, along with loss of stress fibers (23 ± 2 versus 15 ± 2; one-way ANOVA, Fisher's LSD, $P < 0.001$; $n = 40$ cells) (Fig. 6, A and B). In TRPC5-silenced podocytes, synaptopodin abundance and distribution were similar to that of controls, along with the stress fibers (22 ± 3) (Fig. 6, A and B). Gene silencing of TRPC6 resulted in loss of synaptopodin in podocytes, with occasional aggregates noted in the cytoplasm (Fig. 6A). Treatment of TRPC6-depleted cells with CsA restored synaptopodin abundance and rescued stress fiber formation (27 ± 2) (Fig. 6, A and B). Together, these data suggest an association between Ca^{2+} influx through TRPC5 and TRPC6 channels and synaptopodin signaling in podocytes.

Cell migration requires TRPC channel–mediated activation of GTPases

Remodeling of the actin cytoskeleton through Rac1 and RhoA coordinates cell motility (4). Using a wound assay, we thus examined the contribution of TRPC5 and TRPC6 to podocyte migration (32). At 36 hours, podocytes expressing scrambled shRNA had migrated as a sheet of cells to partially close the wound (fig. S8), consistent with recent observations in podocytes (32). At 36 hours, motility of cells expressing DN RhoN19 was similar to that of scrambled shRNA controls (52 ± 6 and 48 ± 3 migrating cells; one-way ANOVA, Fisher's LSD, $P < 0.001$; $n = 30$ images) (Fig. 7, A and B). In contrast, DN RacN17 and CA RhoV14 reduced migration into the wound (4 ± 1 and 8 ± 1, $n = 30$ images) (Fig. 7, A and B). CA RacV12 restored cell migration into the wound (63 ± 2, $n = 30$ images; Fig. 7, A and B). TRPC5-silenced podocytes and podocytes expressing dominant-negative TRPC5 were unable to migrate into the wound, consistent with a contractile cell phenotype (2 ± 1 and 5 ± 2, $n = 30$ images) (Fig. 7, A and B), whereas TRPC6-silenced cells and cells expressing dominant-negative TRPC6 showed increased motility (56 ± 2 and 60 ± 2, $n = 30$ images) (Fig. 7, A and B). DN RhoN19, CA RacV12, and wild-type C5 induced previously

stationary TRPC5-depleted cells to readily migrate into the wound (55 ± 7, 74 ± 4, and 62 ± 8, *n* = 30 images) (Fig. 7, A and B). In contrast, DN RacN17, CA RhoV14, and wild-type C6 impaired the migration of TRPC6-depleted podocytes (2 ± 1, 7 ± 2, and 2 ± 1, *n* = 30 images) (Fig. 7, A and B).

Finally, to determine whether the observed TRPC–Rho GTPase coupling is a conserved mechanism underlying the regulation of actin dynamics, we investigated the role of TRPCs in cell migration in fibroblasts. Gene expression of TRPC5 and TRPC6 was confirmed by RT-PCR (fig. S2H). At 24 hours, DN RhoN19 and CA RacV12 had stimulated fibroblast migration into the wound (162 ± 5 and 158 ± 5, *n* = 35 images) (Fig. 8, A and B), whereas DN RacN17 and CA RhoV14 had attenuated it (24 ± 2 and 19 ± 2; one-way ANOVA, Fisher's LSD, $P < 0.001$; *n* = 35 images) (Fig. 8, A and B). TRPC5-silenced cells were unable to drive wound closure (22 ± 3, *n* = 35 images) (Fig. 8, A and B). Overexpression of DN RhoN19 and CA RacV12 in TRPC5-depleted fibroblasts induced cell migration into the wound (116 ± 9 and 128 ± 9, *n* = 35 images) (Fig. 8, A and B). In keeping with our findings in podocytes, TRPC6-silenced fibroblasts showed significantly increased motility relative to TRPC5-depleted cells (171 ± 11 versus 22 ± 3, *n* = 35 images) (Fig. 8, A and B). DN RacN17 and CA RhoV14 impaired the ability of TRPC6-silenced fibroblasts to migrate into the wound (25 ± 1 and 19 ± 4, *n* = 35 images) (Fig. 8, A and B). Together, these data suggest that the functional connection between TRPC5 and Rac1 activity, and between TRPC6 and RhoA activity, is a conserved mechanism for Ca^{2+}-mediated regulation of actin remodeling and cell migration.

DISCUSSION

The present study identified antagonistic, mutually inhibitory signaling pathways triggered by AT1R-mediated TRPC5 and TRPC6 channel activity. Our data reveal TRPC5 and TRPC6 as antagonistic regulators of Rac1 and RhoA activity in fibroblasts and kidney podocytes, thereby controlling the balance between a motile and a contractile phenotype (fig. 8C). Gene silencing of TRPC6 resulted in loss of stress fibers, activation of Rac1, and increased motility, which was rescued by constitutively active RhoA. In contrast, gene silencing of TRPC5 resulted in enhanced stress fiber formation, activation of RhoA, and decreased motility, which was reversed by constitutively active Rac1. These data unveil an integrated relationship between these TRPC channels and Rac1 and RhoA: TRPC5 and TRPC6 sense and transduce an external stimulus (Ang II) into an intracellular signal (Ca^{2+}) that stimulates the cytoskeletal effectors Rac1 and RhoA, respectively.

Recent studies have offered insight into spatially and temporally regulated Ca^{2+} microdomains, and new techniques have allowed the detection of real-time Rho GTPase activity in migrating cells (5–7). TRPC5 promotes neuronal cell motility and dominant-negative TRPC5 inhibits vascular smooth muscle cell migration (8,13). TRPC6 can inhibit endothelial cell migration through signaling to RhoA (49). Our data extend these findings by demonstrating the cross talk between pathways linking a unique Ca^{2+} sensor (TRPC5 or TRPC6) to a distinct effector (Rac1 or RhoA), thereby allowing the cell to adapt its actin cytoskeleton to cues in the environment.

GPCR signaling promotes TRPC6 channel insertion into the plasma membrane in endothelial cells (50,51). Ca^{2+} influx through TRPC6 can promote TRPC5 channel translocation to the plasma membrane (14). Receptor-mediated insertion of TRPC5 into the plasma membrane depends on Rac1 (12), and our results are consistent with these findings. TRPC6 is the predominant TRPC channel in the plasma membrane of unstimulated podocytes; this is not affected by Ang II or losartan, thereby maintaining a RhoA-predominant, contractile cytoskeletal apparatus. This notion is supported by the single-

channel data showing a predominance of TRPC6 activity in cells expressing constitutively active RhoA. RhoA had no effect on the dynamics of channel insertion into the membrane, as shown in biotinylation studies. In contrast, constitutively active Rac1 promoted the Ang II–mediated increase in plasma membrane abundance of TRPC5 relative to TRPC6.

The interdependence between TRPC5 and Rac1 activities raises the intriguing possibility of a positive feedback loop: Constitutively active Rac1 reverses the TRPC5-depleted phenotype, suggesting that Rac1 not only promotes channel localization to the membrane (12) but also acts in turn as a TRPC5 effector. The presence of TRPC5 and Rac1 in the same biochemical complex and the enhanced TRPC5 channel activity in podocytes expressing constitutively active Rac1 provide a molecular explanation for the specificity of signaling between TRPC5 and Rac1. Rac1 mediates TRPC5 channel insertion from a vesicular pool into the cell membrane (12). This in turn enables enhanced TRPC5-mediated Ca^{2+} influx, thereby triggering the activation of Rac1. The cycle may be terminated when the Ca^{2+} signal decreases, perhaps due to depletion of TRPC5-containing vesicles or channel inactivation.

TRPC5 gene silencing correlated with a restoration of stress fibers in podocytes, reminiscent of losartan treatment. This suggests that under physiologic conditions, podocytes display a contractile phenotype mediated by TRPC6-RhoA signaling and that unopposed TRPC5 activity leads to a maladaptive Rac1-mediated migratory phenotype. This concept is supported by the observation that Rho guanosine diphosphate (GDP) dissociation inhibitor α knockout (Arghdia$^{-/-}$) mice develop heavy albuminuria, which has been attributed to increased Rac1 signaling in podocytes (35). Thus, TRPC5-Rac1 signaling appears to cause podocyte damage and protein-uria, and TRPC5 may therefore provide a target for antiproteinuric therapies.

An adaptive role for the TRPC6-RhoA signaling complex is supported by work showing that synaptopodin protects RhoA from proteasomal degradation, thereby preserving stress fibers in vitro and safeguarding against proteinuria in mice (30,32). The preservation of synaptopodin abundance in TRPC5-depleted cells and the CsA-mediated rescue of synaptopodin in TRPC6-depleted cells suggest that synaptopodin is downstream of TRPC5 and TRPC6.

TRPC5 has been implicated in blood pressure regulation, vascular smooth muscle cell motility, and cardiac hypertrophy (13,19). TRPC6 activity has been linked to pulmonary arterial hypertension (15), cardiac hypertrophy, and fibrosis (16–19). TRPC6 gain-of-function mutations contribute to progressive human proteinuric kidney disease through disrupted podocyte function, suggesting that increased TRPC6 current is detrimental to podocytes (20,21,52). Based on our results, it is tempting to speculate that an unopposed or overactive TRPC6-RhoA pathway may tip the balance too far in favor of a contractile phenotype. Podocytes that are too “stiff” may have trouble adapting to cues in their environment, ultimately resulting in a disrupted cytoskeleton, disassembly of the stress fiber network, and cell death. TRPC6 overexpression in podocytes results in loss of stress fibers (52), which phenocopies the silenced TRPC6 morphology. These observations are in keeping with neuronal plasticity models, where either increased or decreased activity of Ca^{2+}-conducting channels can ultimately have the same effect on the cytoskeleton, resulting in the weakening or pruning of a synaptic contact (53).

A fundamental question in cell biology is how the specificity of a signal is secured. Here, we show that TRPC5-Rac1 and TRPC6-RhoA are spatially, biochemically, and functionally segregated in distinct molecular complexes, mediating a conserved signaling cross talk in podocytes and fibroblasts. Together, the selective coupling of each TRPC channel to a distinct Rho GTPase ensures the specificity of the Ca^{2+} signal. In conclusion, our data

unveil a conserved signaling mechanism for the integrated regulation of actin dynamics and cell motility by antagonistic Ca^{2+} influx pathways.

MATERIALS AND METHODS

Reagents

All the reagents used in this study, unless otherwise stated, were from Sigma-Aldrich.

Podocyte cell culture

Wild-type mouse podocytes (passages 7 to 18) derived from the Immortomouse stably expressing the temperature-sensitive simian virus 40 T antigen were provided by P. Mundel (Massachusetts General Hospital, Boston) and cultured as previously described (48). Briefly, podocytes were plated on collagen-coated cell culture dishes [type I collagen (100 μg/ml), Gibco Invitrogen] and maintained at 33°C in 5% CO_2 in RPMI 1640 medium supplemented with 10% heat-inactivated fetal bovine serum (FBS), penicillin (100 U/ml), streptomycin (100 μg/ml), and interferon-γ (IFN-γ; 100 U/ml). Under these permissive culture conditions, the podocytes remain in an undifferentiated, replication-competent state. Podocytes were thermoshifted to 37°C and maintained in IFN-γ–free culture medium to induce growth arrest and differentiation. Podocyte-specific markers for differentiation are apparent within 7 days of culture under these nonpermissive conditions. Immortalized mouse podocytes stably expressing the Ang II type 1 receptor were cultured in RPMI 1640 supplemented with G418 (250 μg/ml) as described (37).

Lentivirus construction and shRNA-mediated gene silencing

Podocytes were exposed to lentivirus encoding validated shRNA sequences (Open Biosystems) for 24 hours in cell culture medium supplemented with polybrene (4 μg/ml; Chemicon International). For all experiments, parallel infections with the enhanced GFP virus in the VVPW vector, scrambled shRNA, or polybrene alone were used as control. All experiments were performed at least 48 hours after infection of podocytes that were thermo-shifted 5 to 7 days before the assay. Lentiviral particles pseudotyped with the vesicular stomatitis virus glycoprotein (VSV-G) were constructed according to the manufacturer's protocol. Briefly, low-passage HEK293T cells were transfected with the pLKO.1 plasmid encoding the shRNA, the packaging plasmid pMDG.2 ΔR8.91, and the envelope plasmid pCMV-VSV-G at a ratio of 10:10:1 with the Mirus Trans-IT LT-1 transfection reagent. Enhanced GFP encoded in the pLVX vector was used to assess transfection efficiency. The medium was replaced with the virus harvest media 18 hours after transfection, and viral particles were collected twice at 24-hour intervals thereafter. The TRPC5 and TRPC6 shRNA consisted of three pooled shRNA constructs from the RNAi Consortium library of the Harvard–Massachusetts Institute of Technology Broad Institute that were screened on the basis of knockdown efficiency. The TRPC5 hairpin sequences are CCGG**CCTGGCAACTATTTCCCTGAA***CTCGAG*TT-CAGGGAAATAGTTGCCAGGTTTTTG, CCGG**GCAATCAAATAC-CACCAGAAA***CTCGAG*TTTCTGGTGGTATTTGATTGCTTTTTG, and CCGG**CCCAAGTCATTTCTATACCTT***CTCGAG*AAGGTATAG-AAATGACTTGGGTTTTTG. The TRPC6 hairpin sequences are CCGG**GCTCATTATATCCTGGGTAAT***CTCGAG*ATTACCCAG-GATATAATGAGCTTTTTG, CCGG**CGTTCTGTATGGTGTCTA-TAA***CTCGAG*TTATAGACACCATACAGAACGTTTTTG, and CCGG**CGTCCAAATCTCAGCCGTTTA***CTCGAG*TAAACGGCT-GAGATTTGGACGTTTTTG. Viral stocks ($<1 \times 10^6$ transducing units per milliliter) were used at a multiplicity of infection of 5 to 7.5. For overexpression studies, lentivirus particles encoding TRPC5, TRPC6, Rac1, and RhoA complementary DNAs (cDNAs) in the VVPW

plasmid were produced in HEK293T by cotransfection with the packaging and envelope plasmids at a ratio of 3:2:1.

RT-PCR

Total RNA was extracted from podocytes with the Aurum Miniprep Kit (Bio-Rad). mRNA was reverse-transcribed using the Omniscript RT (Qiagen) with oligo(dT) primers. Expression levels of the TRPC channels were detected by three-step PCR using two independent sets of sequence-specific forward and reverse oligos. PCR products were obtained with the Phusion DNA Polymerase (Finnzymes) at the optimized thermocycling conditions (40 cycles of 98°C, 5-s denaturation; 69°C, 30-s annealing; 72°C, 30-s extension) and visualized in a 1.2% agarose gel. Transcript abundance for β-actin was assayed in parallel as a control.

GTPase activation assay and Western blots

Serum-starved cells were exposed to Ang II for 3 hours and washed twice with phosphate-buffered saline (PBS). Cells were scraped into ice-cold radioimmunoprecipitation assay buffer supplemented with protease inhibitors (Roche) and the phosphatase blockers NaF and Na_3VO_4 and lysed on ice for 30 min. Lysates were clarified by centrifugation at 13,000*g* for 15 min at 4°C and the total protein content was measured by bicinchoninic acid (BCA) assay (Pierce). Total protein (25 μg) was resolved in 4 to 12% bis-tris gels (Invitrogen) and electrotransferred to polyvinylidene difluoride membranes. Membranes were probed with primary antibodies directed against Rac1 or RhoA (Cell Biolabs), GFP, or β-actin. For Rho GTPase activation assays, 500 μg of total protein from HEK293T lysates was incubated with Rhotekin- or PAK1-conjugated agarose beads (Cell Biolabs) for 1 hour at 40°C. Activated, GTP-bound forms of Rho, Rac1, and Cdc42 were recovered in lysis buffer by boiling and resolved in bis-tris gels as described above.

Biotinylation assay

Cell surface biotinylation was performed by standard methods. Intact HEK293T cells were washed with PBS^{2+} (1.0 mM $MgCl_2$ and 0.1 mM $CaCl_2$) kept at 4°C, labeled with membrane-impermeant Sulfo-NHS-SS-Biotin (1 mg/ml; Pierce) twice for 15 min, and quenched with 100 mM glycine twice for 15 min. Cells were lysed in buffer containing 200 mM NaCl, 20 mM Hepes, 5 mM EDTA, 1% Triton X-100 (Sigma), and protease inhibitor cocktail (Roche), and total protein was quantitated by BCA assay (Pierce). Total protein (150 mg) was precipitated with streptavidin agarose beads (Pierce). Biotinylated proteins were eluted with 1× LDS Loading Buffer (Invitrogen) + 100 mM dithiothreitol (DTT). Eluted proteins and whole lysates (60 mg) were resolved on a 10% NuPAGE gel and Western-blotted against a GFP epitope (rabbit antibody against GFP, Santa Cruz Biotechnology). To control for membrane integrity and visualize transfected constitutively active GTPase constructs, we subsequently probed blots with a second antibody (rabbit antibody against Rac1 or mouse antibody against RhoA, Santa Cruz Biotechnology).

Immunocytochemistry, wound-healing assays, and confocal imaging

Podocytes were seeded in collagen-coated coverslips (12 mm) to 80% confluence and infected with lentivirus as described. The cells were washed twice with ice-cold PBS and fixed with 4% paraformaldehyde (Electron Microscopy Sciences) in PBS for 1 hour before permeabilization with 0.2% Triton X-100. For wound-healing assays, podocytes or Swiss 3T3 fibroblasts cultured in monolayers were serum-starved for 3 hours before an artificial wound was made with a sterile 100-μl polypropylene pipette tip (2-μm outer diameter). Cells were either directly fixed ($t = 0$) or replaced in complete medium for migration assays before fixation at various time points. Nonspecific immunoreactivity was blocked with 3%

bovine serum albumin. For double immunostaining, podocytes were incubated with antibodies to paxillin (Chemicon International) and detected with Alexa Fluor 488– and 594–conjugated secondary antibodies (Molecular Probes). Actin structures were labeled with Alexa Fluor 594–conjugated phalloidin. The TRPC5 antibody was from NeuroMab and was used at a concentration of 1:50. The TRPC6 antibody (Alomone Labs) was used at a concentration of 1:50. Positive and negative controls for the specificity of these antibodies are shown in fig. S5B. Antibodies to Rac1 or RhoA (Santa Cruz Biotechnology) were used at the manufacturer's recommended concentrations. Pharmacologic agents used were losartan (200 nM) and cyclosporine (500 μg/ml).

Quantification methods

We included three to five independent trials for each experimental condition, where more than 50 cells were counted in each trial in 5 to 10 independent images per trial. Stress fibers were counted manually in each individual cell in independent images. A stress fiber was defined as a phalloidin-positive structure that was represented by a line spanning the length of the cell. "Broken" lines and "arcs" were not counted as stress fibers. For the quantification of puncta in Fig. 4, images were collected at random from areas of the membrane where clear antibody staining was visualized, and the numbers of puncta per standard membrane length (50 μm) were counted with ImageJ software. Image analysis was performed in ImageJ or Adobe Photoshop for Mac OS X. Confocal images were acquired with a Zeiss upright confocal microscope. Images from an optical slice of ~1 to 5 μm were acquired at a resolution of 1200 pixels per inch (ppi) with Zeiss Pascal software.

Statistical analysis

Statistical significance was evaluated by one-way ANOVA with Fisher's LSD test or Student's *t* test unless otherwise stated. $P < 0.05$ was considered significant. Values are reported as mean ± SEM unless otherwise noted.

Calcium imaging

The nonratiometric, cell-permeable Ca^{2+} indicator Fluo-3 (Molecular Probes) was used in all experiments. Fluo-3 (2 μM) was loaded for 20 min at 37°C in podocytes grown to 90% confluence on collagen-coated coverslips. Podocytes were serum-starved for 3 hours, and the Ca^{2+} indicator was subsequently loaded directly into serum-free media. After the 20-min incubation, cells were washed three times with PBS, and the coverslip was placed in the recording chamber in the presence of extracellular bath solution containing 0 or 2 mM $CaCl_2$ with or without Ang II (500 nM). Images were acquired at 2-s intervals. Fluorescence intensity was normalized to maximal fluorescence obtained at the end of each experiment by the application of 100 μM ionomycin, based on the formula, $F = [F_{max}$ (angiotensin) − $F_{min}]/[F_{max}$ (ionomycin) − $F_{min}]$. Measurements were analyzed with Metamorph Software, ClampFit software, and Microsoft Excel.

Electrophysiology

Patch-clamp electrophysiology (Axopatch 200B amplifier, Axon Instruments) was performed in the whole-cell configuration or on outside-out patches. Briefly, fully differentiated podocytes were plated on glass coverslips at low density and placed in the recording chamber. Patch pipettes with resistances of 3 to 4 megohms were pulled from borosilicate glass with a P-97 puller (Sutter Instruments) and filled with a solution containing 135 mM CH_3SO_3Cs, 10 mM CsCl, 3 mM MgATP, 0.2 mM NaGTP, 0.2 mM EGTA, 0.13 mM $CaCl_2$, and 10 mM Hepes (pH 7.3) with CsOH. The bath solution contained 135 mM CH_3SO_3Na, 5 mM CsCl, 2 mM $CaCl_2$, 1 mM $MgCl_2$, 10 mM Hepes, and 10 mM glucose (pH 7.4) with NaOH. Angiotensin (500 nM) and $LaCl_3$ (100 μM) were

applied to the bath solution. Whole-cell currents were recorded from −100 to 100 mV voltage ramps over 150 ms and a holding potential of zero. For single-channel recordings in the outside-out configuration, we used a voltage step protocol from −100 to +100 mV delivered at 20-mV intervals and a holding potential of −60 mV. Average pipette resistance filled with pipette solution was 5 to 10 megohms. Data were sampled at 10 kHz and filtered at 5 kHz. Single-channel data were further off-line filtered at 500 Hz before analysis. In single-channel traces, currents were idealized with a manually defined amplitude criterion to assign ion channel opening and closing transitions. Ensemble averages were expressed as open channel probabilities (average current divided by unitary current amplitude and number of channels in each patch) and plotted as histograms. All data were acquired at room temperature and analyzed with pClamp 10 (Axon Instruments).

Supplementary Material

Refer to Web version on PubMed Central for supplementary material.

Acknowledgments

We thank M. Ross and L. Gusella for the VVPW/BE plasmid and lentivirus expertise; S. Sever for HEK293T cells, the pLKO.1-encoded scrambled shRNA, pCMV–VSV-G, and pMDG.2-ΔR8.91 plasmids; A. Tanger for Swiss 3T3 cells; J. Cook for the rat AT1R plasmid; and K. Tarabanis and K. Liang for technical assistance. We also thank M. A. Arnaout, D. Clapham, and I. Drummond for thoughtful comments on this manuscript.

Funding: This work was supported by a Young Investigator Grant from the NephCure Foundation and NIH grant DK083511 (both to A.G.).

REFERENCES AND NOTES

1. Clapham DE. Calcium signaling. Cell. 2007; 131:1047–1058. [PubMed: 18083096]
2. Collins SR, Meyer T. Calcium flickers lighting the way in chemotaxis? Dev Cell. 2009; 16:160–161. [PubMed: 19217416]
3. Aspenström P, Fransson A, Saras J. Rho GTPases have diverse effects on the organization of the actin filament system. Biochem J. 2004; 377:327–337. [PubMed: 14521508]
4. Etienne-Manneville S, Hall A. Rho GTPases in cell biology. Nature. 2002; 420:629–635. [PubMed: 12478284]
5. Pertz O, Hodgson L, Klemke RL, Hahn KM. Spatiotemporal dynamics of RhoA activity in migrating cells. Nature. 2006; 440:1069–1072. [PubMed: 16547516]
6. Machacek M, Hodgson L, Welch C, Elliott H, Pertz O, Nalbant P, Abell A, Johnson GL, Hahn KM, Danuser G. Coordination of Rho GTPase activities during cell protrusion. Nature. 2009; 461:99–103. [PubMed: 19693013]
7. Wei C, Wang X, Chen M, Ouyang K, Song LS, Cheng H. Calcium flickers steer cell migration. Nature. 2009; 457:901–905. [PubMed: 19118385]
8. Greka A, Navarro B, Oancea E, Duggan A, Clapham DE. TRPC5 is a regulator of hippo-campal neurite length and growth cone morphology. Nat Neurosci. 2003; 6:837–845. [PubMed: 12858178]
9. Ramsey IS, Delling M, Clapham DE. An introduction to TRP channels. Annu Rev Physiol. 2006; 68:619–647. [PubMed: 16460286]
10. Clapham DE. TRP channels as cellular sensors. Nature. 2003; 426:517–524. [PubMed: 14654832]
11. Montell C. TRP channels in *Drosophila* photoreceptor cells. J Physiol. 2005; 567:45–51. [PubMed: 15961416]
12. Bezzerides VJ, Ramsey IS, Kotecha S, Greka A, Clapham DE. Rapid vesicular translocation and insertion of TRP channels. Nat Cell Biol. 2004; 6:709–720. [PubMed: 15258588]
13. Xu SZ, Muraki K, Zeng F, Li J, Sukumar P, Shah S, Dedman AM, Flemming PK, McHugh D, Naylor J, Cheong A, Bateson AN, Munsch CM, Porter KE, Beech DJ. A sphingosine-1-phosphate-activated calcium channel controlling vascular smooth muscle cell motility. Circ Res. 2006; 98:1381–1389. [PubMed: 16675717]

14. Chaudhuri P, Colles SM, Bhat M, Van Wagoner DR, Birnbaumer L, Graham LM. Elucidation of a TRPC6-TRPC5 channel cascade that restricts endothelial cell movement. Mol Biol Cell. 2008; 19:3203–3211. [PubMed: 18495872]
15. Yu Y, Fantozzi I, Remillard CV, Landsberg JW, Kunichika N, Platoshyn O, Tigno DD, Thistlethwaite PA, Rubin LJ, Yuan JX. Enhanced expression of transient receptor potential channels in idiopathic pulmonary arterial hypertension. Proc Natl Acad Sci USA. 2004; 101:13861–13866. [PubMed: 15358862]
16. Nishida M, Onohara N, Sato Y, Suda R, Ogushi M, Tanabe S, Inoue R, Mori Y, Kurose H. Gα12/13-mediated up-regulation of TRPC6 negatively regulates endothelin-1-induced cardiac myofibroblast formation and collagen synthesis through nuclear factor of activated T cells activation. J Biol Chem. 2007; 282:23117–23128. [PubMed: 17533154]
17. Onohara N, Nishida M, Inoue R, Kobayashi H, Sumimoto H, Sato Y, Mori Y, Nagao T, Kurose H. TRPC3 and TRPC6 are essential for angiotensin II-induced cardiac hypertrophy. EMBO J. 2006; 25:5305–5316. [PubMed: 17082763]
18. Kuwahara K, Wang Y, McAnally J, Richardson JA, Bassel-Duby R, Hill JA, Olson EN. TRPC6 fulfills a calcineurin signaling circuit during pathologic cardiac remodeling. J Clin Invest. 2006; 116:3114–3126. [PubMed: 17099778]
19. Wu X, Eder P, Chang B, Molkentin JD. TRPC channels are necessary mediators of pathologic cardiac hypertrophy. Proc Natl Acad Sci USA. 2010; 107:7000–7005. [PubMed: 20351294]
20. Winn MP, Conlon PJ, Lynn KL, Farrington MK, Creazzo T, Hawkins AF, Daskalakis N, Kwan SY, Ebersviller S, Burchette JL, Pericak-Vance MA, Howell DN, Vance JM, Rosenberg PB. A mutation in the TRPC6 cation channel causes familial focal segmental glomerulosclerosis. Science. 2005; 308:1801–1804. [PubMed: 15879175]
21. Reiser J, Polu KR, Moller CC, Kenlan P, Altintas MM, Wei C, Faul C, Herbert S, Villegas I, Avila-Casado C, McGee M, Sugimoto H, Brown D, Kalluri R, Mundel P, Smith PL, Clapham DE, Pollak MR. TRPC6 is a glomerular slit diaphragm-associated channel required for normal renal function. Nat Genet. 2005; 37:739–744. [PubMed: 15924139]
22. Somlo S, Mundel P. Getting a foothold in nephrotic syndrome. Nat Genet. 2000; 24:333–335. [PubMed: 10742089]
23. Faul C, Asanuma K, Yanagida-Asanuma E, Kim K, Mundel P. Actin up: Regulation of podocyte structure and function by components of the actin cytoskeleton. Trends Cell Biol. 2007; 17:428–437. [PubMed: 17804239]
24. Verma R, Kovari I, Soofi A, Nihalani D, Patrie K, Holzman LB. Nephrin ectodomain engagement results in Src kinase activation, nephrin phosphorylation, Nck recruitment, and actin polymerization. J Clin Invest. 2006; 116:1346–1359. [PubMed: 16543952]
25. Verma R, Wharram B, Kovari I, Kunkel R, Nihalani D, Wary KK, Wiggins RC, Killen P, Holzman LB. Fyn binds to and phosphorylates the kidney slit diaphragm component Nephrin. J Biol Chem. 2003; 278:20716–20723. [PubMed: 12668668]
26. Tryggvason K, Patrakka J, Wartiovaara J. Hereditary proteinuria syndromes and mechanisms of proteinuria. N Engl J Med. 2006; 354:1387–1401. [PubMed: 16571882]
27. Tryggvason K, Pikkarainen T, Patrakka J. Nck links nephrin to actin in kidney podocytes. Cell. 2006; 125:221–224. [PubMed: 16630808]
28. Jones N, Blasutig IM, Eremina V, Ruston JM, Bladt F, Li H, Huang H, Larose L, Li SS, Takano T, Quaggin SE, Pawson T. Nck adaptor proteins link nephrin to the actin cytoskeleton of kidney podocytes. Nature. 2006; 440:818–823. [PubMed: 16525419]
29. Hunt JL, Pollak MR, Denker BM. Cultured podocytes establish a size-selective barrier regulated by specific signaling pathways and demonstrate synchronized barrier assembly in a calcium switch model of junction formation. J Am Soc Nephrol. 2005; 16:1593–1602. [PubMed: 15843471]
30. Faul C, Donnelly M, Merscher-Gomez S, Chang YH, Franz S, Delfgaauw J, Chang JM, Choi HY, Campbell KN, Kim K, Reiser J, Mundel P. The actin cytoskeleton of kidney podocytes is a direct target of the antiproteinuric effect of cyclosporine A. Nat Med. 2008; 14:931–938. [PubMed: 18724379]

31. Takeda T, McQuistan T, Orlando RA, Farquhar MG. Loss of glomerular foot processes is associated with uncoupling of podocalyxin from the actin cytoskeleton. J Clin Invest. 2001; 108:289–301. [PubMed: 11457882]
32. Asanuma K, Yanagida-Asanuma E, Faul C, Tomino Y, Kim K, Mundel P. Synaptopodin orchestrates actin organization and cell motility via regulation of RhoA signalling. Nat Cell Biol. 2006; 8:485–491. [PubMed: 16622418]
33. Huber TB, Kwoh C, Wu H, Asanuma K, Godel M, Hartleben B, Blumer KJ, Miner JH, Mundel P, Shaw AS. Bigenic mouse models of focal segmental glomerulosclerosis involving pairwise interaction of CD2AP, Fyn, and synaptopodin. J Clin Invest. 2006; 116:1337–1345. [PubMed: 16628251]
34. Kos CH, Le TC, Sinha S, Henderson JM, Kim SH, Sugimoto H, Kalluri R, Gerszten RE, Pollak MR. Mice deficient in α-actinin-4 have severe glomerular disease. J Clin Invest. 2003; 111:1683–1690. [PubMed: 12782671]
35. Shibata S, Nagase M, Yoshida S, Kawarazaki W, Kurihara H, Tanaka H, Miyoshi J, Takai Y, Fujita T. Modification of mineralocorticoid receptor function by Rac1 GTPase: Implication in proteinuric kidney disease. Nat Med. 2008; 14:1370–1376. [PubMed: 19029984]
36. Yanagida-Asanuma E, Asanuma K, Kim K, Donnelly M, Young Choi H, Hyung Chang J, Suetsugu S, Tomino Y, Takenawa T, Faul C, Mundel P. Synaptopodin protects against proteinuria by disrupting Cdc42:IRSp53:Mena signaling complexes in kidney podocytes. Am J Pathol. 2007; 171:415–427. [PubMed: 17569780]
37. Hsu HH, Hoffmann S, Endlich N, Velic A, Schwab A, Weide T, Schlatter E, Pavenstadt H. Mechanisms of angiotensin II signaling on cytoskeleton of podocytes. J Mol Med. 2008; 86:1379–1394. [PubMed: 18773185]
38. Strübing C, Krapivinsky G, Krapivinsky L, Clapham DE. Formation of novel TRPC channels by complex subunit interactions in embryonic brain. J Biol Chem. 2003; 278:39014–39019. [PubMed: 12857742]
39. Hofmann T, Obukhov AG, Schaefer M, Harteneck C, Gudermann T, Schultz G. Direct activation of human TRPC6 and TRPC3 channels by diacylglycerol. Nature. 1999; 397:259–263. [PubMed: 9930701]
40. Strübing C, Krapivinsky G, Krapivinsky L, Clapham DE. TRPC1 and TRPC5 form a novel cation channel in mammalian brain. Neuron. 2001; 29:645–655. [PubMed: 11301024]
41. Blair NT, Kaczmarek JS, Clapham DE. Intracellular calcium strongly potentiates agonist-activated TRPC5 channels. J Gen Physiol. 2009; 133:525–546. [PubMed: 19398778]
42. Trebak M, Lemonnier L, DeHaven WI, Wedel BJ, Bird GS, Putney JW Jr. Complex functions of phosphatidylinositol 4,5-bisphosphate in regulation of TRPC5 cation channels. Pflugers Arch. 2009; 457:757–769. [PubMed: 18665391]
43. Lievremont JP, Numaga T, Vazquez G, Lemonnier L, Hara Y, Mori E, Trebak M, Moss SE, Bird GS, Mori Y, Putney JW Jr. The role of canonical transient receptor potential 7 in B-cell receptor-activated channels. J Biol Chem. 2005; 280:35346–35351. [PubMed: 16123040]
44. Zeng F, Xu SZ, Jackson PK, McHugh D, Kumar B, Fountain SJ, Beech DJ. Human TRPC5 channel activated by a multiplicity of signals in a single cell. J Physiol. 2004; 559:739–750. [PubMed: 15254149]
45. Jung S, Muhle A, Schaefer M, Strotmann R, Schultz G, Plant TD. Lanthanides potentiate TRPC5 currents by an action at extracellular sites close to the pore mouth. J Biol Chem. 2003; 278:3562–3571. [PubMed: 12456670]
46. Freichel M, Vennekens R, Olausson J, Stolz S, Philipp SE, Weissgerber P, Flockerzi V. Functional role of TRPC proteins in native systems: Implications from knockout and knock-down studies. J Physiol. 2005; 567:59–66. [PubMed: 15975974]
47. Hofmann T, Schaefer M, Schultz G, Gudermann T. Subunit composition of mammalian transient receptor potential channels in living cells. Proc Natl Acad Sci USA. 2002; 99:7461–7466. [PubMed: 12032305]
48. Mundel P, Heid HW, Mundel TM, Krüger M, Reiser J, Kriz W. Synaptopodin: An actin-associated protein in telencephalic dendrites and renal podocytes. J Cell Biol. 1997; 139:193–204. [PubMed: 9314539]

49. Singh I, Knezevic N, Ahmmed GU, Kini V, Malik AB, Mehta D. $G\alpha_q$-TRPC6-mediated Ca^{2+} entry induces RhoA activation and resultant endothelial cell shape change in response to thrombin. J Biol Chem. 2007; 282:7833–7843. [PubMed: 17197445]

50. Cayouette S, Bousquet SM, Francoeur N, Dupré E, Monet M, Gagnon H, Guedri YB, Lavoie C, Boulay G. Involvement of Rab9 and Rab11 in the intracellular trafficking of TRPC6. Biochim Biophys Acta. 2010; 1803:805–812. [PubMed: 20346379]

51. Cayouette S, Lussier MP, Mathieu EL, Bousquet SM, Boulay G. Exocytotic insertion of TRPC6 channel into the plasma membrane upon G_q protein-coupled receptor activation. J Biol Chem. 2004; 279:7241–7246. [PubMed: 14662757]

52. Möller CC, Wei C, Altintas MM, Li J, Greka A, Ohse T, Pippin JW, Rastaldi MP, Wawersik S, Schiavi S, Henger A, Kretzler M, Shankland SJ, Reiser J. Induction of TRPC6 channel in acquired forms of proteinuric kidney disease. J Am Soc Nephrol. 2007; 18:29–36. [PubMed: 17167110]

53. Holtmaat A, Svoboda K. Experience-dependent structural synaptic plasticity in the mammalian brain. Nat Rev Neurosci. 2009; 10:647–658. [PubMed: 19693029]

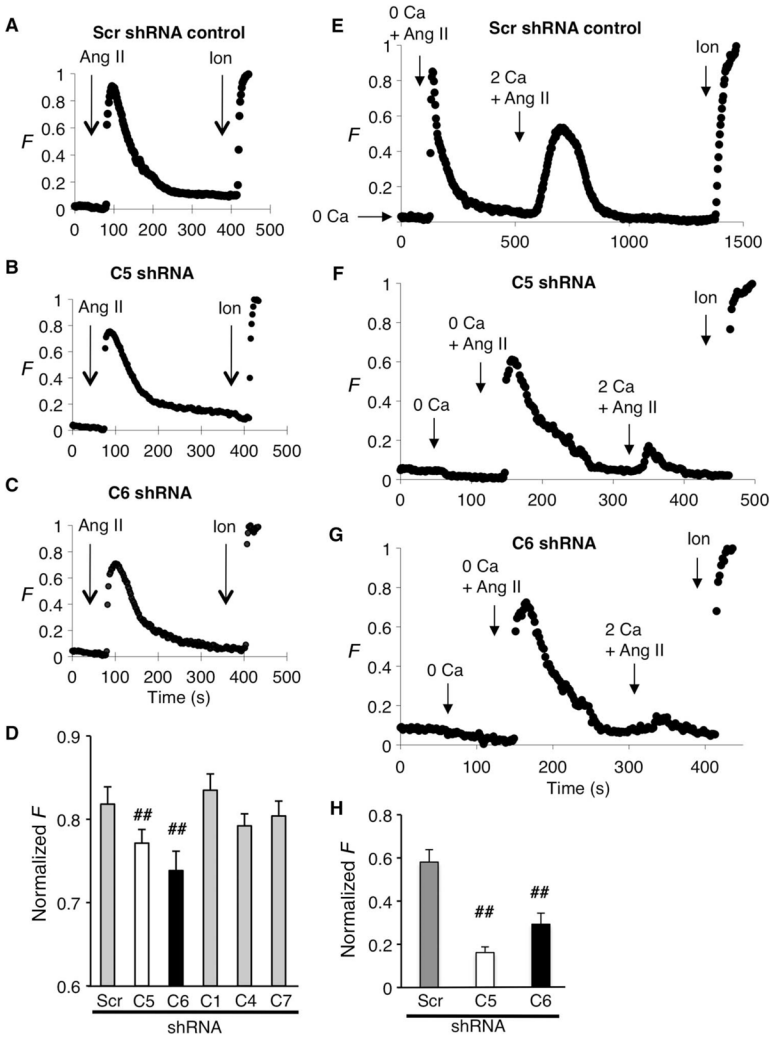

Fig. 1.

Ang II–evoked TRPC5 and TRPC6 activation contributes to intracellular Ca^{2+} transients in podocytes. Fluo-3 Ca^{2+} imaging in AT1R podocytes revealed Ca^{2+} transients in response to Ang II (500 nM) with (2 mM) or without Ca^{2+} (0 mM + 5 mM EGTA). Ionomycin(Ion)was added to the bath at the end of the experiment. (**A** to **C**) Normalized fluorescence amplitude in response to Ang II application (*F*) in podocytes expressing either scrambled (Scr) (A), C5 (B), or C6 shRNA (C). (**D**) Group data summary (mean ± SD). Gene silencing of TRPC5 (*n* = 34) and TRPC6 (*n* = 29), but not of TRPC1 (*n* = 15), TRPC4 (*n* = 26), or TRPC7 (*n* = 42), significantly decreased the amplitude of Ca^{2+} transient. (**E** to **G**) Representative traces in Ca^{2+} add-back experiments. A proportion of AT1R podocytes responded to a second application of Ang II within the 10-min recording period. (F) Gene silencing of TRPC5 (*n* = 5) or TRPC6 (*n* = 18) compared to Scr shRNA control (*n* = 16), significantly reduced Ca^{2+} influx in response to Ang II. (**H**) Group data in Scr controls, C5, and C6 knockdown cells (mean ± SE) ($^{\#\#}P < 0.01$).

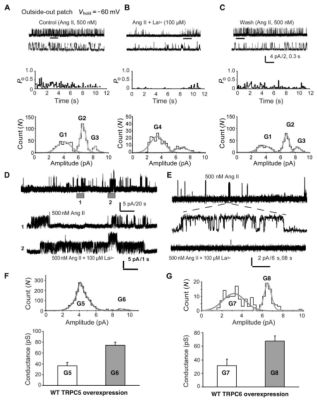

Fig. 2.

TRPC5- and TRPC6-like single-channel recordings in podocytes. (**A** to **C**) Upper panels: Single-channel current traces in the outside-out configuration in AT1R podocytes (V_{hold}, −60 mV). At V_{step} +100 mV, application of Ang II (500 nM) to the bath evoked single-channel openings (A). This single-channel activity was suppressed by 100 μM La^{3+} (B) in a reversible manner (C). The upper panel lower trace is the expansion of the black bar region in the upper trace. The middle panel shows frequency histograms of single-channel open probability P_o (bin size, 0.1 s) under each condition. The lower panel is the single-channel amplitude frequency distribution histogram from which single-channel conductance was calculated from the fitted curve. The unitary conductances were (G1) 39 pS, (G2) 68 pS, (G3) 80 pS, and (G4) 33 pS. (**D**) Representative outside-out single-channel recording traces in AT1R podocytes overexpressing WT TRPC5. The upper panel shows a continuous outside-out patch recording at +100 mV. (1) 500 nM Ang II, (2) 500 nM Ang II + 100 μM La^{3+}. Application of Ang II evoked TRPC5 channel openings (middle panel) enhanced by application of La^{3+} (lower panel). (**E**) Representative outside-out single-channel recordings from AT1R podocytes overexpressing WT TRPC6. Ang II evoked TRPC6 single-channel activity (upper and middle panels), suppressed by La^{3+} (lower panel). (**F** and **G**) Amplitude frequency distribution histograms (upper panel) and summary of single-channel conductances (lower panel) of TRPC5 (n = 8, mean ± SD) and TRPC6 patches (n = 9, mean ± SD), respectively. The single-channel conductance average was (G5) 37 pS, (G6) 74 pS (due to current summation of two TRPC5 channel openings), (G7) 35 pS, and (G8) 70 pS (due to summation of two TRPC6 channel openings).

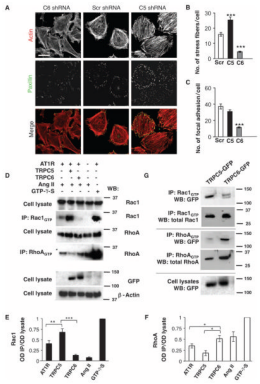

Fig. 3.

Ang II–induced TRPC5 and TRPC6 activation has antagonistic effects on the actin cytoskeleton. (**A**) TRPC6-depleted AT1R podocytes (C6 shRNA) showed loss of stress fibers after Ang II treatment. Paxillin staining was also reduced compared to scrambled shRNA controls (Scr shRNA). TRPC5-depleted AT1R podocytes (C5 shRNA) had increased stress fibers and paxillin-positive structures throughout the cytoplasm. Scale bar, 20 μm. (**B**) Quantification of stress fibers in AT1R cells. (**C**) TRPC6-depleted cells had significantly reduced focal contacts compared to Scr shRNA controls and TRPC5-depleted cells. (**D** to **F**) Functional coupling of TRPC5 to Rac1 and TRPC6 to RhoA. (D) GTPase activity assay in HEK293 cells. Ang II increased Rac1-GTP abundance in cells coexpressing TRPC5-GFP and AT1R (lane 2), but reduced Rac1-GTP in cells coexpressing TRPC6-GFP and AT1R (lane 3) (Rac1 and RhoA). Ang II treatment increased RhoA-GTP abundance in TRPC6/AT1R cells (lane 3), but reduced RhoA-GTP in TRPC5/AT1R cells (lane 2). Data are normalized to total cell lysate Rac1 and RhoA abundance (lanes 1 to 5). Guanosine 5′-*O*-(3′-thiotriphosphate) (GTP-γ-S)–loaded cells served as a positive control (lane 5). Non–AT1R-expressing HEK cells showed no Rac1 activity (lane 4). TRPC5-GFP and TRPC6-GFP expression was confirmed by blotting with antibody against GFP (lanes 2 and 3) (TRPC5-GFP and TRPC6-GFP). (E and F) Quantification of activity assays (one-way ANOVA, Newman-Keuls multiple comparison test, $P < 0.001$; $n = 4$ trials). (**G**) Coimmunoprecipitation experiments in HEK cells expressing TRPC5-GFP or TRPC6-GFP. TRPC5 coimmunoprecipitated more robustly with endogenous activated Rac1 compared to TRPC6 (upper panel). In contrast, TRPC6 coimmunoprecipitated more robustly with endogenous activated RhoA compared to TRPC5 (middle panel). TRPC5-GFP and TRPC6-GFP were detected in cell lysates (lower panel) (*$P < 0.05$; **$P < 0.01$; ***$P < 0.001$). WB, Western blot; IP, immunoprecipitation; OD, optical density.

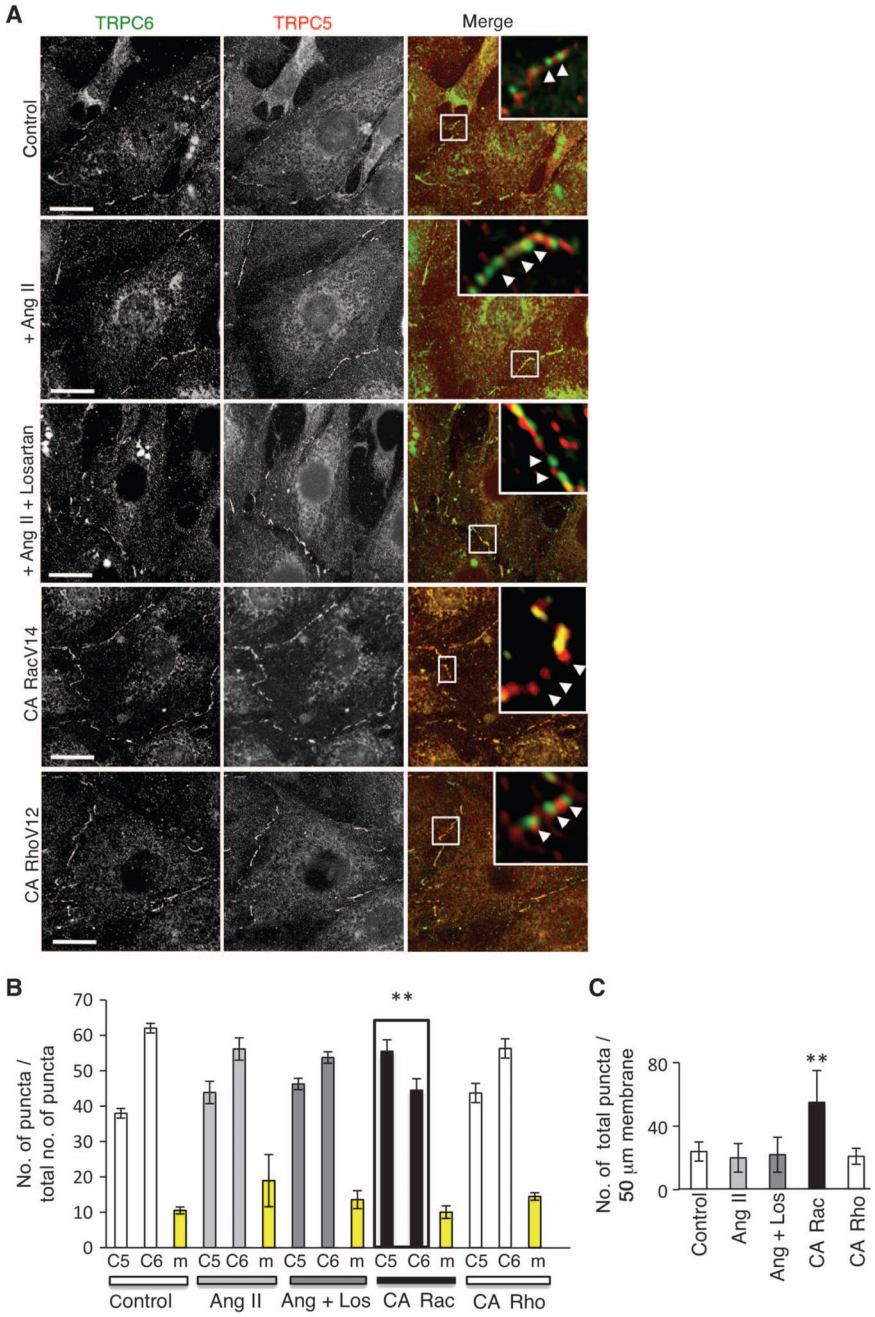

Fig. 4.

Membrane localization of TRPC5 and TRPC6 in podocytes. (**A**) TRPC6 and TRPC5 immunocytochemistry in AT1R podocytes reveals punctate structures on the cell membrane and a granular distribution in the cytoplasm. Merged images and high-power insets (×63) reveal that TRPC6-labeled puncta are distinct from TRPC5 puncta, with exceptions indicated in yellow. In untreated controls, TRPC6 puncta (green) represent >60% of total puncta on the cell membrane compared to >35% for TRPC5. This pattern persists after Ang II or losartan treatment. In the presence of CA RacV14, the pattern changes, with 60% of membrane puncta represented by TRPC5 (red). In the presence of CA RhoV12 the pattern returns to baseline, with TRPC6-labeled puncta predominance. Scale bar, 10 μm. (**B**)

Quantification of puncta normalized to the total number of puncta visualized. m, merged. (**C**) Quantification of total puncta per standardized membrane length (50 μm) reveals significantly increased membrane insertion of puncta only in the presence of CA RacV14. Ang II did not result in a statistically significant increase in the number of puncta on the cell membrane (**$P < 0.01$).

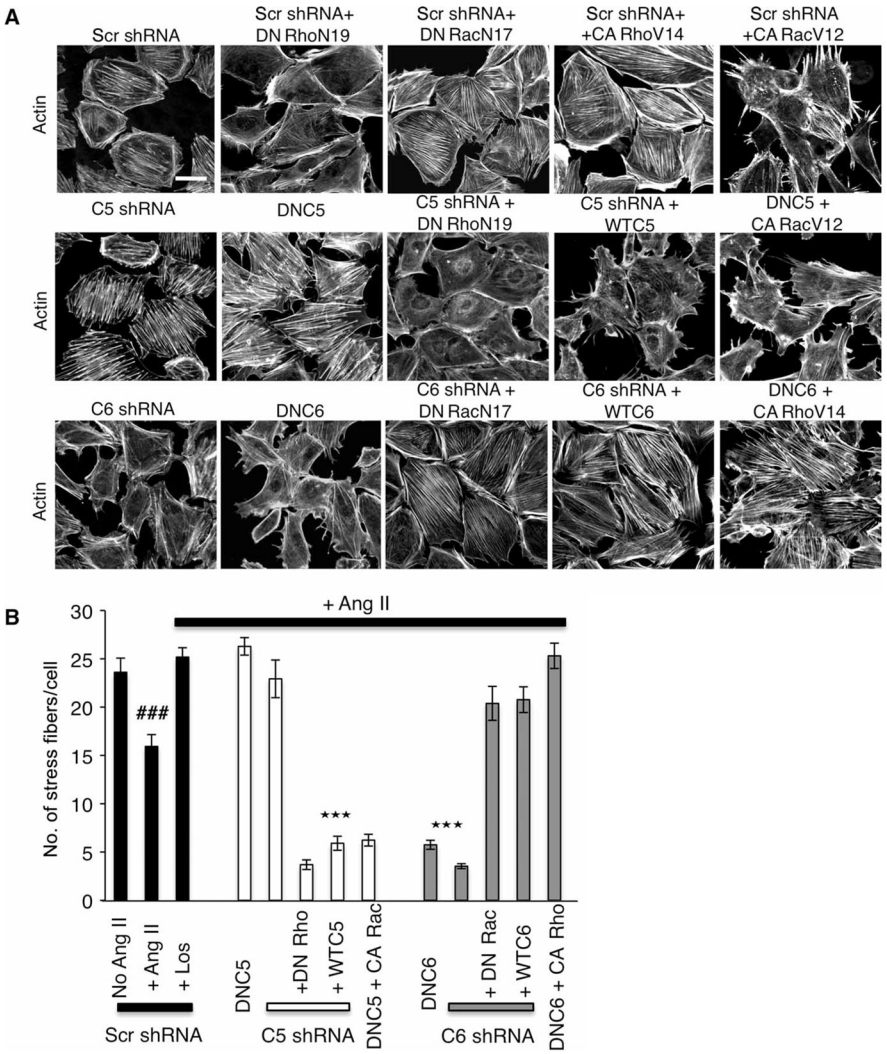

Fig. 5.

Functional coupling of TRPC5 to Rac1 and TRPC6 to RhoA. (**A**) DN RhoN19 abolished stress fibers. DN RacN17 and CA RhoV14 rescued stress fiber formation. In contrast, CA RacV12 abolished stress fibers and allowed the formation of prominent ruffles and filopodia. Scale bar, 20 μm. Ang II–treated AT1R podocytes expressing TRPC5 shRNA or dominant-negative TRPC5 (DNC5) displayed prominent stress fibers. DN RhoN19 or wild-type TRPC5 (WTC5) abrogated stress fibers in TRPC5-depleted cells. CA RacV12 reversed the DNC5 phenotype. Ang II–treated podocytes over-expressing TRPC6 shRNA or dominant-negative TRPC6 (DNC6) displayed loss of stress fibers. DN RacN17 promoted stress fiber and actin arc formation in C6 shRNA cells. Restoration of TRPC6 in the background of C6 shRNA [C6 shRNA + wild-type (WT) C6] also restored actin arc and stress fiber formation. CA RhoV14 rescued stress fibers in DNC6 cells. Scale bar, 20 μm. (**B**) Quantification of stress fibers in podocytes (see text for details) ($^{###}P < 0.001$, statistically significant decrease in the number of stress fibers between no Ang II/scrambled shRNA controls and Losartan-treated/scrambled shRNA controls versus Ang II–treated/scrambled shRNA controls; $^{***}P < 0.001$).

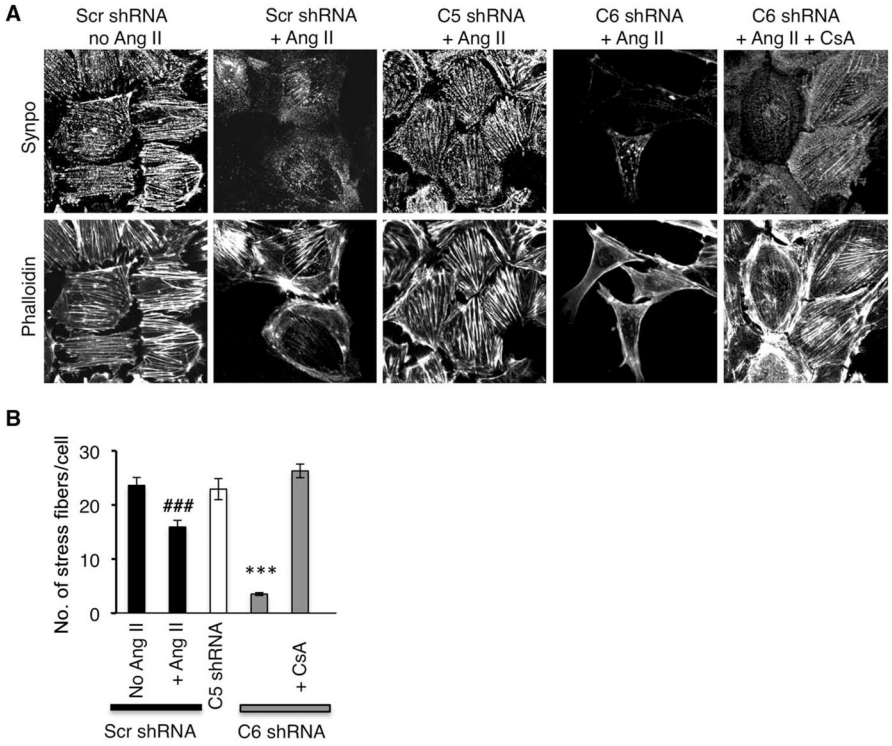

Fig. 6.

Synaptopodin degradation in TRPC6-depleted podocytes is rescued by CsA. (**A**) Serum-starved Scr shRNA control cells display prominent synaptopodin staining along the stress fibers. Treatment of serum-starved podocytes with Ang II results in actin arc formation and loss of stress fibers and synaptopodin staining. TRPC5-depleted cells display prominent stress fibers and synaptopodin staining. In contrast, stress fibers and synaptopodin staining are abrogated in TRPC6-depleted cells, where synaptopodin aggregates in clumps throughout the cytoplasm. Treatment of TRPC6-depleted cells with CsA (500 ng/ml) rescues stress fiber formation and restores synaptopodin staining along the stress fibers. (**B**) Quantification of stress fibers in CsA-treated TRPC6-depleted cells compared to the other conditions (see text for details) ($^{###}P < 0.001$; $^{***}P < 0.001$).

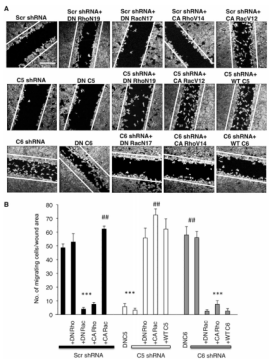

Fig. 7.

TRPC5 promotes and TRPC6 inhibits podocyte migration. (**A**) Wound assays at 36 hours. In control Scr shRNA AT1R podocytes, DN RhoN19 induced modest cell migration into the wound, whereas DN RacN17 abrogated migration. CA RhoV14 cells displayed minimal migration, whereas CA RacV12 cells displayed robust migration across the wound. TRPC5-depleted cells and dominant-negative TRPC5-expressing podocytes showed attenuated migration. DN RhoN19 or CA RacV12 promoted migration of TRPC5-depleted cells. Reconstitution of wild-type TRPC5 channels in a C5 shRNA background also induce robust migration into the wound. TRPC6-depleted cells and dominant-negative TRPC6-expressing cells showed increased migration into the wound. DN RacN17, CA RhoV14, or WT TRPC6 on a C6 shRNA background reduced migration. Scale bar, 1 mm. (**B**) Quantification of migrating podocytes (see text for details) (***$P < 0.001$; $^{\#\#}P < 0.01$ compared to Scr shRNA podocytes).

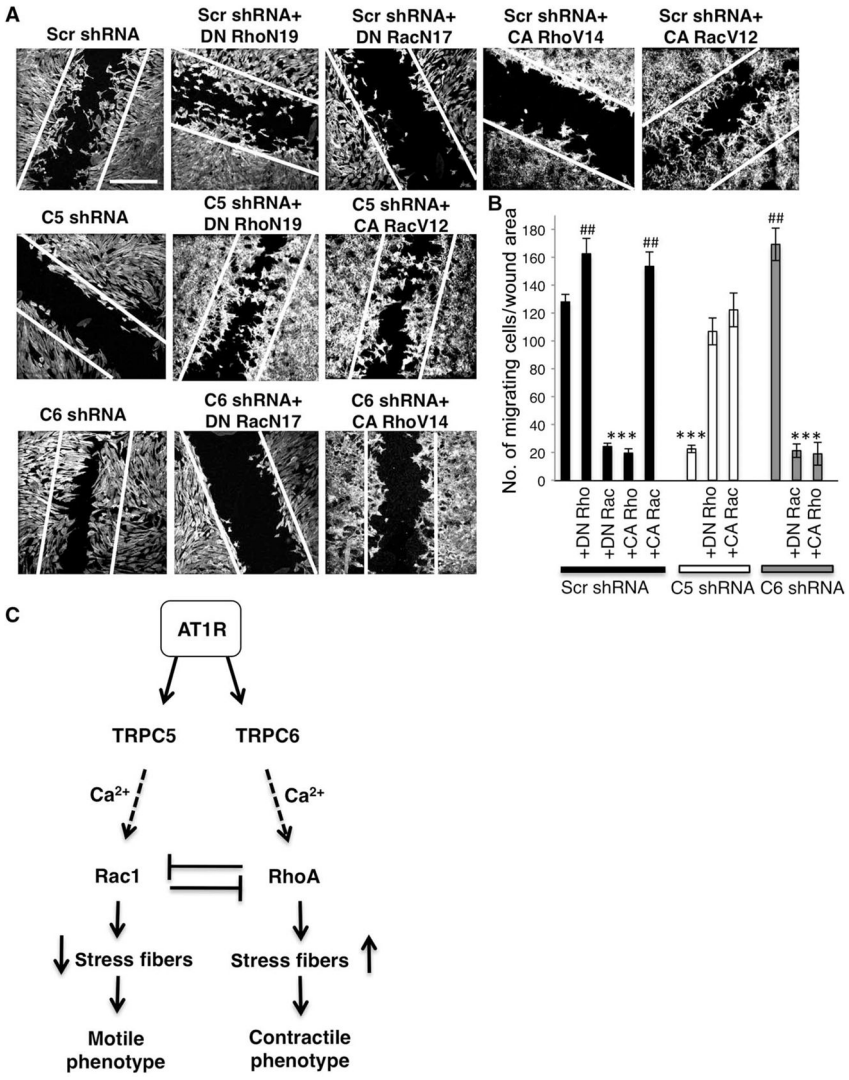

Fig. 8.

Antagonistic regulation of cell migration by TRPC5 and TRPC6. (**A**) TRPC5 promotes and TRPC6 inhibits fibroblast migration. Control Scr shRNA–expressing cells showed serum-induced migration within 24 hours. Similarly, DN RhoN19 induced fibroblast migration, whereas DN RacN17 and CA RhoV12 abrogated migration. Migration was enhanced by CA RacV12. DN RhoN19 or CA RacV12 restored migration in TRPC5-depleted fibroblasts. In contrast, TRPC6-depleted cells showed increased cell migration relative to controls, which was abrogated by DN RacN17 and CA RhoV14. Scale bar, 1 mm. (**B**) Quantification of migrating fibroblasts (see text for details) (***$P < 0.001$; $^{\#\#}P < 0.01$). (**C**) A model for the conserved roles of TRPC5 and TRPC6 in the regulation of actin dynamics and cell motility. Under physiologic conditions, stimulation of AT1R activates both TRPC6 and TRPC5 channels, allowing the influx of Ca^{2+}, thereby promoting activation of RhoA and Rac1, which are mutually inhibitory. Activation of the TRPC5-Rac1 complex inhibits RhoA and mediates stress fiber disassembly, thus promoting cell motility. In contrast, activation of the TRPC6-RhoA complex inhibits Rac1 activity and promotes stress fiber formation, thus mediating a contractile cell phenotype.